Improved Artificial Electric Field Algorithm Based on Multi-Strategy and its Application

Yongqing Tian[1], Libo Liu[1]*, Xiaolei Wang[1], Lin Dong[1], Rana Gill[2], Ravi Tomar[3]

[1]College of Civil Engineering, Hebei University of Engineering, Handan, Hebei, 056038, China
[2]Department of AIT-CSE, Chandigarh University, Mohali, Punjab-140413, India
[3]Persistent Systems, India

E-mail: yongqingtian2@126.com, liboliu7@163.com, xiaoleiwang8@126.com, lindong811@163.com, rana.cse@cumail.in, ravitomar7@gmail.com

Keywords: Intelligent optimization algorithm; Artificial electric field algorithm; Opposition-based learning strategy; Chaotic search; Greedy strategy; Sand liquefaction evaluation

Received: January 22, 2022

Artificial electric field algorithm is a new swarm bionic optimization algorithm, which uses the interaction force of charged particles to create a mathematical model to solve the problem. To improve the global exploration ability and local development ability of artificial electric field algorithms, an artificial electric field algorithm based on opposition learning is proposed. The chaos strategy is used to strengthen the quality of the initial population, and the opposition learning strategy is used to increase the diversity of the population and the development ability of the algorithm. The excellent performance of the algorithm is proved by simulation experiments. The improved artificial electric field algorithm is combined with SVM to construct the sand liquefaction identification model by selecting seven measured indexes, including intensity, underground water level, overlying effective pressure, standard penetration hit number, average particle size, non-uniformity coefficient, and shear stress ratio. Compared with traditional methods such as the standard method and seed simplification method, the results show that the IAEFA-SVM model has high prediction accuracy and provides an effective method for sand liquefaction identification.

Povzetek: Predstavljen je izboljšan algoritem umetnega električnega polja na osnovi mnogoterih strategij.

1 Introduction

The artificial electric field algorithm (AEFA) is a new intelligent optimization algorithm proposed by Indian scholar Anita in 2019 [1]. Anita's intelligent optimization algorithm, which is inspired by Coulomb's law of static electricity, has the characteristics of fewer parameters, lower computational complexity, better scalability, exploitability, and many others. However, it is easy to get into the local optimum and lacks exploration.

To improve the performance of AEFA, Aysen [2] integrated the opposition-based learning strategy into the initialization and updating process of AEFA and proposed the oppositional learning-based AFEA (OBAEFA), which improved the exploring ability of AEFA. Anita [3-4] and others extend the AEFA algorithm for constrained optimization by introducing new velocity and location constraints. The existence of boundary allows particles to interact within the scope of the problem, and to learn from each other in the problem space. The introduction of the strategy makes a better balance effect on the exploration and development of the algorithm. In the following study, Anita extends the artificial electric field algorithm with combinatorial higher-order graph matching problems and introduces the discrete artificial electric field algorithm. The framework combines redefinition of location, speed representation, use of addition and subtraction, updating rules for speed and location, and initialization of specific problems with heuristic information [5, 6]. The algorithm is proved to be superior to other existing algorithms in matching degree and accuracy [7].

To improve the exploratory ability of AEFA and solve the problem of easily falling into local optimal solution, the AFEA is improved in the following aspects:

i. The chaotic technique is introduced into the AEFA, and the initial population is generated in the search space by the randomness and universality of the chaotic motion, and the probability of finding the optimal solution is increased.

ii. The diversity of the population is maintained and the possibility of jumping out of the local optimum is improved by the opposite learning strategy.

iii. The greedy strategy is used to get the optimal value of the population quickly. Then, through the simulation of 9 test functions, the IAEFA algorithm is

compared with other improved algorithms to verify its effectiveness of the IAEFA algorithm.

Finally, the improved artificial electric field algorithm, in combination with the support vector machine (SVM) is applied for the identification of sand liquefaction and the results are compared with the traditional method of identification of sand liquefaction. This project is not limited to industrial applications but the overall growth of social life with the integration of the Internet of Things, AI, and robotics [8-11].

The rest of this article is organized as: Section 2 presents the principles of the algorithm. Section 3 consists of the information about artificial electric field algorithms based on chaotic learning and opposition-based learning strategy. The results and analysis part is covered in section 4. Section 5 describes several common assessment methods of sand liquefaction. At last, the concluding remarks are presented in Section 6.

2 Principles of the algorithms

2.1 Artificial Electric Field Algorithm (AEFA)

AEFA is inspired by Coulomb's Law of electrostatic force, which states that the force that occurs between charged particles and charged particle is proportional to the product of their charges. The force is also inversely proportional to the square of the distance between the charges, each individual in the population is considered to be a charged particle, their strength is measured by their charge, and the position of the charge corresponds to the solution to the problem, the charge is defined as the fitness value of the candidate solution and the fitness function of the population. In the AEFA algorithm, only the electrostatic gravitation is considered, so that the charged particle with the largest charge ("The best individual") attracts other lower charged particles and moves slowly in the search space. The AEFA shown in Figure 1 can be considered as an isolated system of charges, and the position of the optimal fitness value for any electron i at any time t is given by Equation 1.

$$p_i^d(t+1) = \begin{cases} p_i^d(t), f(p_i(t)) > f(x_i(t+1)) \\ x_i^d(t+1), f(p_i(t)) \le f(x_i(t+1)) \end{cases} \quad (1)$$

The total number of charged particles are denoted by N and the total number of parameters by d. The position of the particle with the best fitness is represented by $p_{best} = x_{best}$ and the force exerted on the particle i at time t by the particle j as shown in Equation 2.

$$F_{ij}^d = k(t)\frac{Q_i(t) \cdot Q_j(t) \cdot (P_j^d(t) - X_i^d(t))}{R_{ij}(t) + \varepsilon} \quad (2)$$

$Q_i(t)$ and $Q_j(t)$ are the charges of the i particle and j particle at arbitrary time t. $k(t)$ is the Coulomb constant of the arbitrary time t. ε is a relatively small random number. $R_{ij}(t)$ is the Euclidean distance between the two particles, represented by the Equation 3.

$$R_{ij}(t) = \|x_i(t), x_d(t)\|_2 \quad (3)$$

$k(t)$ is the number of iterations and the maximum number of iterations, given by the following Equation 4.

$$k(t) = k_0 \cdot e^{\left(\frac{-\alpha \cdot (iter)}{maxiter}\right)} \quad (4)$$

α is the parameter and k_0 is the initial value, $iter$ is the current iteration, and maxiter is the maximum number of iterations. At the beginning of the algorithm, use constant k_0 in a large initial value can make a better exploration. Then it is reduced by iteration to control the search accuracy. The total electric force of the other particles at any time t on particle i is expressed in Equation 5.

$$F_i^d(t) = \sum_{j=1, j \neq i}^{N} rand \cdot F_{ij}^d(t) \quad (5)$$

F_i^d denotes the resultant force acting on the charged particle i in d dimensional at time t. And rand refers to the uniformly generated random number in the range of [0,1]. Random numbers can provide randomness. The electric field of the charged particle i in d dimension at time t is given in Equation 6.

$$E_i^d(t) = \frac{F_i^d(t)}{Q_i(t)} \quad (6)$$

By using Equation 6 and Newton's law, it can be deduced that the particle i has an acceleration at time t in d dimension and expressed in Equation 7.

$$a_i^d(t) = \frac{Q_i(t) \cdot E_i^d(t)}{M_i(t)} \quad (7)$$

$M_i(t)$ denotes the unit mass of a particle i at time t t, the velocity v and position x of the particle are represented by the following Equation 8 and Equation 9 respectively.

$$V_i^d(t+1) = rand \cdot V_i^d(t) + a_i^d(t) \quad (8)$$

$$X_i^d(t+1) = X_i^d(t) + V_i^d(\text{t+1}) \quad (9)$$

$$Q_i(t) = Q_j(t) = \frac{q_i(t)}{\sum_{i=1}^{N} q_i(t)} i, j = 1,2,\cdots N \tag{10}$$

Rand denotes the uniformly generated random numbers in the range of [0,1]. The charge of the particle is calculated according to Equation 10 and it is supposed that each particle has an equal charge.

In Equation 10, $q_i(t)$ denotes the max normalized value ($Q_{best=1}$) of the best particle of the selected suitable charge function, calculated as Equation 11.

$$q_i(t) = e^{\left(\frac{fit_i(t)-worst(t)}{best(t)-worst(t)}\right)} \tag{11}$$

$fit_i(t)$ is the fitness value of particle i at time t. $best(t)$ is the fitness value of the best particle. $worst(t)$ is the fitness value of the worst particle. The minimization problem is defined as the following Equation 12.

$$\begin{aligned} best(t) &= \min\left(fit_i(t)\right), i \in (1,2,\cdots,N) \\ worst(t) &= \max\left(fit_i(t)\right), i \in (1,2,\cdots,N) \end{aligned} \tag{12}$$

The flowchart of the AEFA algorithm is shown in Figure 1. From the flowchart, you can see that the algorithm starts with randomly initializing the particles. Then, for each iteration, the fitness of each particle is evaluated, and the fitness values for the best and worst particles are calculated. In the next iteration, the velocity and position of each particle are updated. This process is repeated until the maximum number of iterations is reached to obtain the optimal solution.

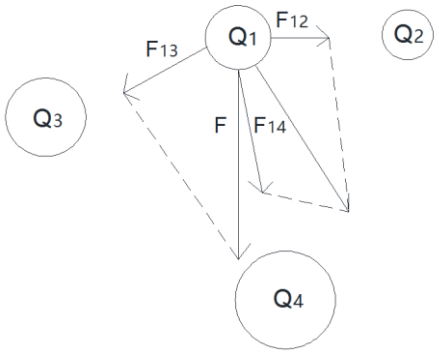

Figure 1: The interaction of particle

2.2 Basic ideas of opposition-based learning strategy

The opposition-based learning strategy was proposed by scholar Tizhoosh [12] in 2005. Compared with other algorithms, it takes time to get the efficiency of the new solution. Genetic algorithms, for example, require several generations or more of algebra to introduce new directions through genetic variation. In recent years opposition-based learning OBL has been effectively applied to various swarm intelligence algorithms. When solving problems, it is considered that there may be a better solution on the opposite side of an ineffective solution. The quality of a population can be improved by introducing opposite solutions rather than two independent random solutions.

If there is a number X on [l, u], then the antithesis of X is defined as $\bar{x} = l + u - x$. Extending the definition of the opposite point to the n-dimensional space, supposing p as a point in the n-dimensional space, where $x_i \epsilon [l, u], \mathrm{i} = 1,2, \ \ldots, \ \mathrm{n}$, the opposite point is $p' = (x_1', x_2', \cdots, x_n')$. Among them, $x_i' = l_i + u_i - x_i$.

Suppose x as a random number on [l, u], $\tilde{x}$ as its reverse solution, $f(x)$ the objective function, $g(\cdot)$ the proper evaluation function. Calculating $f(x)$ and $f(\tilde{x})$ in each iteration, if $g(f(x))$ greater than $g(f(\tilde{x}))$, then retains the value of x and vice versa.

3 Artificial electric field algorithm based on chaotic learning and opposition-based learning strategy

This section includes the discussion of artificial electric field algorithms for chaotic learning and opposition-based learning strategy.

3.1 Basic ideas of the algorithm

For complex optimization problems, especially for multi-modal functions in high latitude, the basic artificial electric field algorithm is easy to get into the local optimal solution, and the ability of global exploration is insufficient. Based on chaos and oppositional learning, a hybrid artificial electric field algorithm (IAEFA) is proposed. In the basic artificial electric field algorithm, the population initialization of the chaotic map sequence and the opposition-based learning strategy is introduced. Below are three areas for improvement.

3.2 The main process of the IAEFA algorithm

3.2.1 Initialization of Chaos method

The process of the initialization of the standard artificial electric field algorithm takes random allocation and can not distribute the population uniformly in the solution domain. Especially when optimizing the multi-peak function of high latitude, the diversity of the population is reduced, causing precocious puberty. At present, the research shows that the variables generated by the logistics chaotic map [13] have strong universality, which can improve the shortage of initial population diversity generated by random allocation.

$$Z_{n+1} = \mu(1 - Z_n) \tag{13}$$

In Equation 13, μ for random numbers between [0, 4]; Z_n for the n[th] chaotic variable, the value range for [0, 1].

3.2.2 Greedy strategy

The matrix P of $M \times N$ can be obtained by the updating the position of particle x in the formula, and P_{ij} denotes the position of particle i in position j.

In the optimal problem, each column of matrix P has only one selected P_{ij}, and the selected P_{ij} is the smallest or smaller value of the column. So greedy strategy is introduced to make a quick selection and the specific steps are as follows:

i. Randomly select column $j\ (l, u)$ as the starting column, and select the minimum value of column j.

ii. From column j forward, select the minimum value of the column that meets the constraint conditions column by column.

iii. From column j backward, select the minimum value of the column that meets the constraint conditions column by column.

3.2.3 Opposition-based learning strategy

The opposition-based learning strategy can expand the searching range of the group, exploit the new searching area, and enhance the diversity of the group. Mixed with the artificial electric field algorithm, it can improve the global search ability of the algorithm and prevent the algorithm from falling into the local optimal solution. Therefore, after population updating, the strategy of oppositional learning is applied to the population.

When the position of particle swarm in n-dimensional space is updated as $x^k = (x_1^k, x_2^k, \cdots, x_n^k)$, the corresponding opposite is the elite opposite $\bar{x}^k = (\bar{x}_1^k, \bar{x}_2^k \cdots \bar{x}_n^k)$, where $\bar{x}_i^k = \gamma * (l_i - u_i) - x_i^k$, $\gamma \in [0,1]$ for the random number under the uniform distribution [14]. The sum of the population x^k and $\bar{x}_i^k$ is merged, and 2N particles are sorted according to the ascending order of fitness value, and the N particles before fitness value are selected as the new particle population.

The basic procedures are described below:

Step 1: Initializes the basic parameter and initial population of the algorithm, determines the particle dimension D, the number of charge Population N, and initializes the position x and velocity v of N particles by logistic chaotic map in a given range.

Step 2: Calculate the fitness value of each charge, calculate the Coulomb constant $k(t)$ of the charge, global optimum $best(t)$, and the worst value $worst(t)$.

Step 3: Calculate the Columbian force and acceleration of the charge. Update the velocity v and the position x.

Step 4: Adopt the opposition-based learning strategy to the renewed x population and select the first n individuals of the fitness.

Step 5: Use a greedy strategy to choose x.

Step 6: Judge whether the convergence condition of the algorithm is satisfied, if the termination condition is not satisfied, then return to Step 2; otherwise, output the optimal solution. End the loop.

4 Results and Analysis

This section illustrates the analysis of results obtained from the comparison of the IAEFA and AEFA algorithms and their comparison with other algorithms.

To verify the effectiveness of the improved basic artificial electric field algorithm, nine standard test functions are used to test its performance, and a comparison between the particle swarm optimization algorithm and the basic artificial electric field algorithm is made. The benchmark functions are shown in Table 1. In addition, comparisons between (IAEFA) with other intelligent algorithms are made. The experimental environment of the algorithm is based on the computer under Windows 7 system, MATLAB simulation platform, Inter Core i7-4720 processor, the main frequency of 2.6 GHz.

To verify the validity of the improved IAEFA, contrast experiments are made based on seven algorithms including the improved IAEFA and PSO, AEFA, literature [2] based on the opposite learning AEFA algorithm, Archimedes optimization algorithm (AOA) [15], Condor algorithm (BES) [16], SSA [17], to guarantee the fairness and validity of the experiment. In the simulation experiment, the initial population and iteration times of each algorithm are set to 30 and 1000; the remaining parameters are suggested in the corresponding reference [18], as shown in Table 2.

4.1 Comparison between IAEFA and AEFA on the performance

Table 3 is the experimental results of the two algorithms running 30 times independently on the 9 test function. The spatial dimension is 30. The evaluation results are from the optimal value, the worst value, the average value, the standard deviation, and the running time, and the optimum values are indicated in bold type [19].

In solving the problem of minimum or maximum, the average value can reflect the searching ability of the algorithm, the best value and the worst value can reflect the quality of the solution, and the standard deviation can reflect the robustness of the algorithm. From Table 3, it can be concluded that the overall optimization ability of IAEFA is better than that of AEFA. In the 9 algorithms, 7 of them searched the theoretical optimum and the quality of the solution is better than that of AEFA. It illustrates that in the global search stage, the chaos strategy is used to ensure the diversity of the population

and enhance the ability of global search [20]. From the average results, the unimodal functions F1, F3, F4, F6, and multimodal functions F7-F9, the average values of IAEFA are all 0, and F8 tends to improve compared with the basic algorithm AEFA. It shows that the accuracy of the algorithm in the late period is further improved by introducing an opposition-based learning strategy and a greedy strategy. From the standard deviation results, we can see that the results of IAEFA are better than that of AEFA. Excluding F2 and F5 test functions, the values of the remaining seven test functions are all 0. IAEFA maintains very good robustness; in terms of the running time of the algorithm, that of IAEFA is slightly longer than that of AEFA due to the addition of more policies, which, in combination with other aspects, is within acceptable limits.

4.2 Comparison between IAEFA and AEFA on the improved algorithm and other algorithms

Table 4 is the experimental results of 6 algorithms running 30 times on 9 test functions independently. The space dimension is set to 30, and the evaluation criteria are mean value and standard deviation. The "-" table does not provide the corresponding data in the references, and the optimal results are expressed in bold.

As can be seen from Table 4, the average values of IAEFA in the unimodal functions F1, F3, F4, F6, and multimodal functions F7, and F9 are all 0. Compared with the other six algorithms, IAEFA is better in the quality of feasible solutions and search precision. There are many local extremum points in function F8, and it is difficult for the algorithm to jump out of the local extremum points in the process of solving. The precision of the improved IAEFA algorithm increased by 15 orders of magnitude compared with AEFA. In the same way, the results of the improved algorithm OBAEFA are relatively good, and the optimal values are found on F7 and F9. Based on the analysis of the standard deviation results, the improved IAEFA algorithms have a standard deviation of 0 in the 7 of the 9 test functions. The results show that the IAEFA algorithm has little fluctuation in the iterative process, and its stability is better than the other 6 algorithms.

The results show that the performance rank of the six algorithms is IAEFA, OBAEFA, BES, AOA and AEFA, PSO. Through the simulation experiment, the effectiveness of the improved algorithm is proved. Finally,
it can be concluded that the improved algorithm IAEFA not only keeps the diversity of the population but also speeds up the convergence speed of the algorithm. To a certain extent, it avoids falling into the local optimal solution and further improves the optimization accuracy of the algorithm.

Types	Functions	Function Expressions	Region of search	Extreme value
Unimodal function	Sphere	$f_1(x)=\sum_{i=1}^{n} x_i^2$	[-100.100]	0
	Quartic	$f_2(x)=\sum_{i=1}^{n} ix_i^4+rand[0,1]$	[-1.28.1.28]	0
	Schwefel2.21	$f_3(x)=max_i\{\lvert x_i\rvert, 1\le i\le n\}$	[-100,100]	0
	Schwefel2.22	$f_4(x)=\sum_{i=1}^{n}\lvert x_i\rvert+\prod_{i=1}^{n}\lvert x_i\rvert$	[-10,10]	0
	Rosenbrock	$f_5(x)=\sum_{i=1}^{n-1}\left[100\left(x_{i+1}-x_i^2\right)^2+(x_i-1)^2\right]$	[-30,30]	0
	Rotator hyper-ellipsoid	$f_6(x)=\sum_{i=1}^{n}([x_i+0.5])^2$	[-100,100]	0
Multimodal function	Griewank	$f_7(x)=\frac{1}{4000}\sum_{i=1}^{n}x_i^2-\prod_{i=1}^{n}\cos\left(\frac{x_i}{\sqrt{i}}\right)+1$	[-600,600]	0
	Ackley	$f_8(x)=-20\exp\left(-0.2\sqrt{\frac{1}{N}\sum_{i=1}^{N}x_i^2}\right)-\exp(\frac{1}{N}\sum_{i=1}^{N}cos(2\pi x_i))+20+e$	[-32,32]	0

Rastrigin	$f_{10}(x) = \sum_{i=1}^{n}\left[x_i^2 - 10\cos^2(2\pi x_i + 10)\right]$	[-5.12,5.12]	0

Table 1: Benchmark test functions

Algorithm	**Parameter**
AEFA	Alfa=30;K0=150;
OB-AEFA	Alfa=30;K0=150;
IAEFA	Alfa=30;K0=150;
PSO	W=0.9;c1c2=2.03;wmin=0.4;
SSA	R1,R2,R3=0-1;
BES	A=10;r=1.5;
AOA	C1=2;c2=6;c3=2;c4=0.5;u=0.9;l=0.1;

Table 2: Specific parameters set by each algorithm

Function	Algorithm	Optimal value	The worst value	Mean value	Standard Deviation	Run time
F1	AEFA	1.24E-23	2.36E+00	2.75E-01	5.63E-01	2.6723
	IEAEFA	**0.00E+00**	**0.00E+00**	**0.00+00**	**0.00E+00**	2.1768
F2	AEFA	4.80E-02	3.42E-01	1.9E-01	8.06E-02	1.8059
	IEAEFA	**4.66E-07**	**6.85E-05**	**2.28E-05**	**2.60E-05**	2.3204
F3	AEFA	2.53E+00	8.57E+00	6.07E+00	1.67E+00	1.7088
	IEAEFA	**0.00E+00**	**0.00E+00**	**0.00E+00**	**0.00E+00**	2.0955
F4	AEFA	1.71E-03	1.82E+01	4.81E+00	4.88E+00	1.784
	IEAEFA	**0.00E+00**	**0.00E+00**	**0.00E+00**	**0.00E+00**	2.107
F5	AEFA	1.53E+02	1.92E+02	1.72E+02	2.73E+01	1.3438
	IEAEFA	**2.85E+01**	**2.86E+01**	**2.86E+01**	**6.38E-02**	1.646
F6	AEFA	5.98E+02	1.94E+03	1.23E+03	3.82E+02	2.052
	IEAEFA	**0.00E+00**	**0.00E+00**	**0.00E+00**	**0.00E+00**	2.4963
F7	AEFA	1.07E+01	3.22E+01	2.18E+01	6.86E+00	1.7691
	IEAEFA	**0.00E+00**	**0.00E+00**	**0.00E+00**	**0.00E+00**	1.8644
F8	AEFA	1.26E-09	1.77E+00	3.71E-01	5.38E-01	1.6274
	IEAEFA	**8.88E-16**	**8.88E-16**	**8.88E-16**	**0.00E+00**	1.6879
F9	AEFA	1.29E+01	4.87E+00	3.11E+01	8.76E+00	1.8159
	IEAEFA	**0.00E+00**	**0.00E+00**	**0.00E+00**	**0.00E+00**	1.8537

Table 3: Experimental results of IAEFA and AEFA

4.3 Comparison between IAEFA, AEFA, OB-AEFA, AOA, BES, and PSO on Convergent curve

According to the average fitness curve, in the unimodal functions F1 and F6, the IAEFA found the theoretical optimum values at about 350 iterations, and for F3, and F4, at about 700 iterations. The other five algorithms are all above IAEFA, the fitness fluctuation value is small, and the theoretical optimum value cannot be found after 1000 iterations. For the function, F8 has many local minimum values and it is easy to get into the local optimum. IAEFA has obtained the theoretical optimal value of about 30 iterations and keeps the state of continuous exploration. Figure 2 to Figure 10 depicts the average fitness curve of function F1, F2, F3, F4, F5, F6, F7, F8, F9 respectively.

For F7, F9, and IAEFA, the convergence speed and the precision are better than those of AEFA, OBAEFA, AOA, BES, and PSO. The effect of the algorithm is remarkable, the convergence curve is always at the bottom, and the theoretical optimal value is found in about 10 iterations. The results show that the algorithm can get the optimal population more quickly in the global search stage and avoid falling into the local optimal solution because of the guidance of the optimal individual in the local search stage. And the convergence speed and accuracy of the algorithm are improved to a great extent.

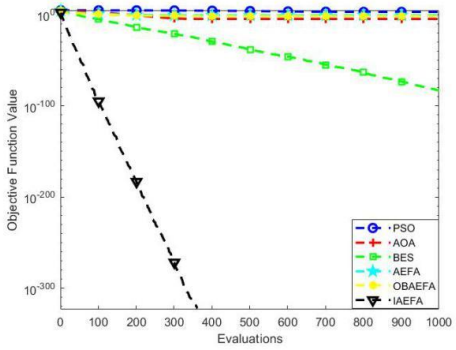

Figure 2: Average fitness curve of function F1

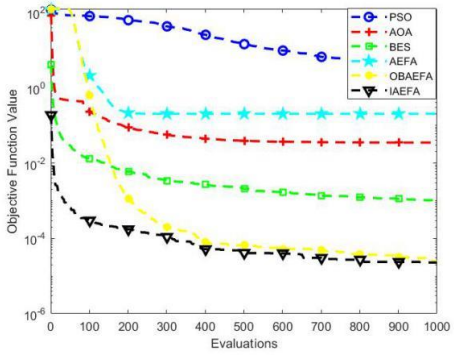

Figure 3: Average fitness curve of function F2

Function		PSO	BES	AOA	SSA	AEFA	OBAEFA	IAEFA
F1	Mean	3.01E-06	3.98E-84	2.11E-05	1.74E-06	2.67E-01	4.59E-02	**0.00E+00**
	Std.dev.	9.15E-06	1.39E-83	1.93E-05	1.05E-06	5.96E-01	2.00E-01	**0.00E+00**
F2	Mean	5.38E+00	1.02E-03	3.48E-02	1.52E-02	2.03E-01	2.39E-05	**2.28E-05**
	Std.dev.	6.66E+00	3.23E-03	1.86E-02	1.13E-02	8.53E-01	5.46E-05	**2.60E-05**
F3	Mean	3.01E+01	6.05E-02	2.79E+00	2.24E-05	6.07E+00	8.66E-01	**0.00E+00**
	Std.dev.	6.42E+00	1.39E-01	1.30E+00	7.80E-06	1.67E+00	4.33E-01	**0.00E+00**
F4	Mean	5.93E+01	8.07E-52	3.33E-04	5.30E-02	4.81E+00	1.61E-14	**0.00E+00**
	Std.dev.	1.89E+01	3.25E-51	2.36E-04	2.33E-01	4.88E+00	1.45E-14	**0.00E+00**
F5	Mean	4.65E+04	1.56E+01	2.80E+01	-	1.72E+02	2.85E+01	**2.82E+01**
	Std.dev.	6.14E+04	2.15E+00	2.13E+00	-	2.73E+01	2.59E-02	**1.38E-02**
F6	Mean	3.40E+04	3.52E-10	5.83E+01	1.40E+02	1.23E+03	6.51E-28	**0.00E+00**
	Std.dev.	1.19E+04	1.93E-09	5.51E+01	1.42E+02	3.82E+02	1.39E-27	**0.00E+00**
F7	Mean	3.01E+01	0.00E+00	1.91E-03	1.58E-02	2.18E+01	0.00E+00	**0.00E+00**
	Std.dev.	4.32E+01	0.00E+00	1.66E-02	1.11E-02	6.86E+00	0.00E+00	**0.00E+00**
F8	Mean	1.59E+01	2.34E-02	1.81E-01	2.16E+00	3.71E-01	4.67E-15	**8.88E-16**
	Std.dev.	7.06E+00	9.99E-02	5.56E-01	6.33E-01	5.38E-01	4.05E-15	**0.00E+00**
F9	Mean	1.58E+02	2.74E+01	2.15E+01	5.21E+01	3.11E+01	0.00E+00	**0.00E+00**
	Std.dev.	2.99E+01	4.91E+01	5.94E+00	1.64E+01	8.76E+00	0.00E+00	**0.00E+00**

Table 4: Performance comparison of IAEFA with modified AEFA and other algorithms

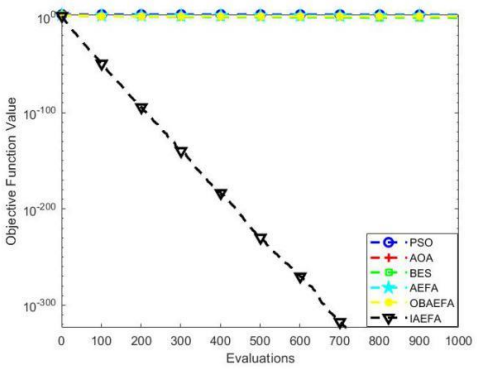

Figure 4: Average fitness curve of function F3

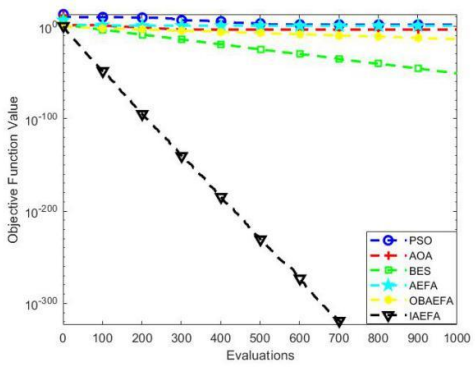

Figure 5: Average fitness curve of function F4

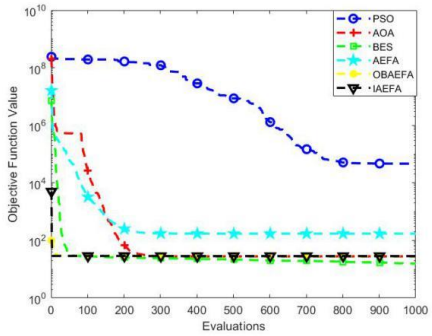

Figure 6: Average fitness curve of function F5

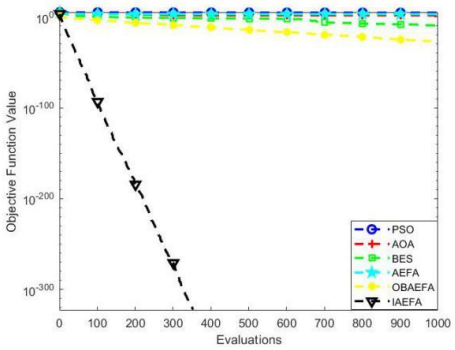

Figure 7: Average fitness curve of function F6

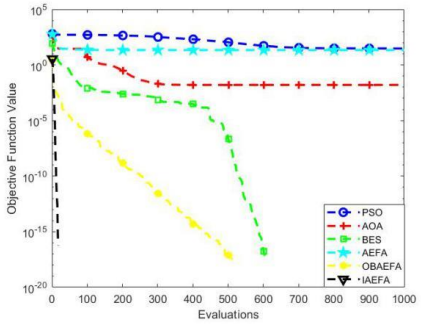

Figure 8: Average fitness curve of function F7

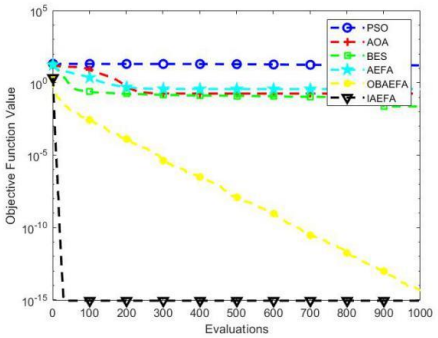

Figure 9: Average fitness curve of function F8

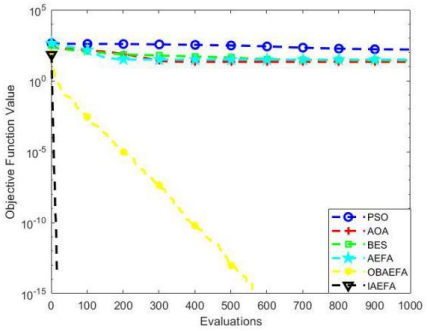

Figure 10: Average fitness curve of function F9

5 Several common assessment methods of sand liquefaction

The influence factors of sand liquefaction can be summed up into three categories [22]. Dynamic load: seismic intensity, duration, seismic wave characteristics, etc.; burial conditions: geological factors, soil depth, groundwater level, etc.; Soil conditions: soil type, particle composition, density, etc. In addition, the site shape, geomorphology, and historical earthquake background also have an impact on the foundation soil liquefaction. A description of the factors is given in Table 5.

According to the analysis method of other scholars [23, 24], seven independent variables are selected among numerous influencing factors according to the seismic liquefaction data set provided by reference [25, 26]. Based on seven characteristic indexes, including intensity $I'(X_1)$, groundwater level $d_w(X_2)$, effective overburden pressure $\sigma_0'(X_3)$, blow counts of SPT $N_{63.5}(X_4)$, average grain size $d_{50}(X_5)$, non-uniformity coefficient $C_u(X_6)$ and shear-to-stress ratio $\tau_d/\sigma_0'(X_7)$, the liquefaction of sandy soil is divided into three grades according to the field conditions. The category set is {non-liquefaction (1), critical liquefaction (2) , obvious liquefaction (3)} . The discriminant results of the IAEFA-SVM model and Code for Seismic Design of Buildings (GB5011- 2010) [27] (hereinafter referred to as "Code") and that of the seed simplification method [28] are compared and analyzed. Raw data are shown in Table 6.

5.1 Critical blow counts of SPT for evaluating liquefaction

In the Code for Seismic Design of Buildings 2010 [28], clause 4.3.4 of the code puts forward the formula for evaluating sand liquefaction, within a depth of 20m below the ground, the critical blow counts of SPT of evaluating liquefaction can be calculated as follows in equation 14.

$$N_{cr} = N_0\beta[\ln(0.6d_s + 1.5) - 0.1d_w]\sqrt{3/\rho_c} \quad (14)$$

In the formula: N_{cr} is the critical value of the blow counts of SPT for evaluating liquefaction; N_0 is the

reference value of the blow counts of SPT for evaluating liquefaction, which can be taken as follows in Table 7. d_s is the depth of penetration point for saturated soil m; d_w is the groundwater level, m; ρ_c is the clay content, when less than 3 or sand is used 3; β is the adjustment factor, the first group takes 0.80, the second group 0.95, and the third group takes 1.05.

5.2 Seed's "simplified procedure"

Seed's "simplified procedure" is the first method proposed abroad to evaluate the liquefaction of saturated sand in a horizontal site [29]. The essence is to compare the Cyclic Resistance Ratio CRR generated by vibration with the Cyclic Stress Ratio CSR to evaluate the liquefaction. The safety factor FS=CRR /CSR, if FS>=1, is judged not to be liquefied, otherwise, it is judged to be liquefied [30].

5.2.1 Cyclic Stress Ratio CSR

The Seed's "simplified procedure" is modified several times, and then converts the cyclic stress ratio into the equivalent CSR7.5 under the magnitude $M_s = 7.5$ after several corrections.

$$CSR_{7.5} = \frac{\tau_d}{\sigma_0'} = 0.65 \times \frac{\alpha_{max}}{g} \times \frac{\sigma_0}{\sigma_0'} \times \gamma_d \quad (15)$$

In the formula, $CSR_{7.5}$ for the earthquake cyclic stress ratio, kPa; τ_d for the average shear stress, kPa; α_{max} for the peak acceleration, m/s^2; g for the gravitational acceleration, m/s^2; σ_0 for the calculated depth of the soil divided by the total vertical stress, kPa; γ_d for the stress reduction factor.

$$\gamma_d = 1.000 - 0.00765z, z \leq 9.15m \quad (16)$$

$$\gamma_d = 1.174 - 0.0267z, 9.15m \leq z \leq 23m \quad (17)$$

z is the depth of the calculated point.

Influencing factor	Description of influencing factors
Dynamic load	When an earthquake is less than magnitude 5, that is, when the epicentral intensity is less than 6, liquefaction will not occur generally [31]. The higher the earthquake intensity, the more serious the sand liquefaction.
Burial conditions	Deeper the sand layer is buried, greater the effective overburden pressure is, and the less easy the sand is to liquefy. The shallower the groundwater is, the smaller the effective pressure is, and the smaller the shear stress is, the easier the sand is to liquefy. The geological factors mainly refer to the geological age and geomorphologic unit. The older the geological age, the better the degree of consolidation, compactness, and structure, and the stronger the anti-liquefaction ability [32-34].
Soil conditions	The average grain size is the main basis for classifying sandy soil, which can reflect the gradation of soil particles. The size of soil particles is related to drainage conditions. The larger the particle size, the less likely it is to liquefy. The non-uniformity coefficient is an index to reflect the uniformity of the composted soil, and it can reflect the gradation of the soil. The well-graded soil has a relatively stable structure, so the well-graded sand is not easy to liquefy [35-37].

Table 5: Factors affecting liquefaction and their description

Serial number	$I(X_1)$	$d_w(X_2)$	$\sigma_0'(X_3)$	$N_{63.5}(X_4)$	$d_{50}(X_5)$	$C_u(X_6)$	$\tau_d/\sigma_0'(X_7)$	Categorization vector
1	7	1.09	50.3	5.0	0.41	2.9	0.1	2
2	7	1.2	34.6	8.0	0.187	4.0	0.09	2
3	7	0.8	20.3	6.0	0.111	2.0	0.08	2
4	7	0.5	21.1	3.0	0.166	1.7	0.1	2
5	7	1.1	42.1	7.0	0.17	1.7	0.1	2
6	7	1.1	71.5	9.0	0.14	2.8	1.11	2
7	7	1.4	55.5	9.0	0.14	1.6	0.1	2

⋮				⋮				⋮
88	8	0.65	57.7	1.1	0.080	1.74	0.234	3
89	9	1.5	76	16.0	0.160	1.80	0.4150	3
90	9	1.45	65.8	5.0	0.055	5.60	0.4070	3

Table 6: Model-training samples

The basic design earthquake acceleration (g)	0.1	0.15	0.2	0.3	0.4
The reference value of the blow counts of SPT for evaluating liquefaction	7	10	12	16	19

Table 7: Reference value of the blow counts of SPT for evaluating liquefaction N_0

5.2.2 Cyclic Resistance Ratio CRR

The cyclic resistance ratio CRR can be calculated from SPT values obtained from standard penetration tests, using the following formula (18):

$$CRR_{7.5} = \frac{1}{34-(N_1)_{60CS}} + \frac{(N_1)_{60CS}}{135} + \frac{50}{[10(N_1)_{60CS}+45]^2} - \frac{1}{200} \tag{18}$$

$$(N_1)_{60CS} = \alpha + \beta(N_1)_{60} \tag{19}$$

Among them:

When $FC \le 5$, $\alpha = 0$, $\beta = 1.0$; when $5 \le FC \le 35$, $\alpha = \exp\left[1.76 - \left(\frac{190}{FC^2}\right)\right]$, $\beta = \left[0.99 - \left(\frac{FC^2}{1000}\right)\right]$; and when $FC \ge 35$, $\alpha = 0.5$, $\beta = 1.2$

$CRR_{7.5}$ for the cyclic resistance ratio, $(N_1)_{60CS}$ for the corrected blow counts of SPT, FC for the fines content, $(N_1)_{60}$ for the modified blow counts of SPT when the overburden load is 100kpa and the energy transfer efficiency is 60%.

$$(N_1)_{60} = C_N \cdot N \tag{20}$$

$$C_N = \sqrt{100/\sigma_0'} \tag{21}$$

In the formula, N is the actual blow count; $C_N$is the adjusted factor of overburden pressure, when C_N is less than 0,4, it takes 0.4, when it is more than 2, takes 2. σ_0' is the effective overburden pressure.

5.3 IAEFA-SVM Model

Support Vector Machine [38-40] is a machine learning approach proposed by Vapnik that has been widely used to analyze and identify patterns. Optimal Separate Hyperplane (Optimum Separate Hyperplane,

OSH) is obtained by using the training set to split the data into two categories to obtain the data categories. As shown in Figure 11 below.

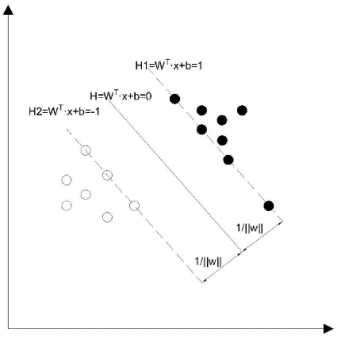

Figure 11: Support vector machine and Optimal Separating Hyperplane

The problem of solving in a linear Support vector machine can be translated into the following problem solving:

$$\min_{w,b,\xi} \frac{1}{2}\|w\|^2 + C\sum_{i=1}^{N}\xi_i \tag{22}$$

$$s.t.\, y_i(w \cdot x_i + b) \ge 1 - \xi_i, i = 1,2,\cdots,N \tag{23}$$

$$\xi_i \ge 0, i = 1,2,\cdots,N \tag{24}$$

w is the normal vector of the hyperplane, b is the classification threshold, $\xi_i \ge 0$ is the introduced slack variable, and C is the penalty factor. The size of C indicates the size of the misclassification penalty. The optimal decision function is obtained by the Lagrange multiplier:

$$f(x) = sign[y_i a_i (x \cdot x_i + b)] \tag{25}$$

The nonlinear problem is transformed into a linear problem by being transformed into a high-dimensional space to solve the problem of surface classification. Finally, the optimal decision function becomes:

$$f(x) = sign[\sum_{i=1}^{N} y_i a_i k(x \cdot x_i) + b] \quad (26)$$

Where $k(x \cdot x_i)$ is the kernel function.

$$k(x \cdot x_i) = \exp\left(-\frac{\|x - x_i\|^2}{2\sigma^2}\right) \quad (27)$$

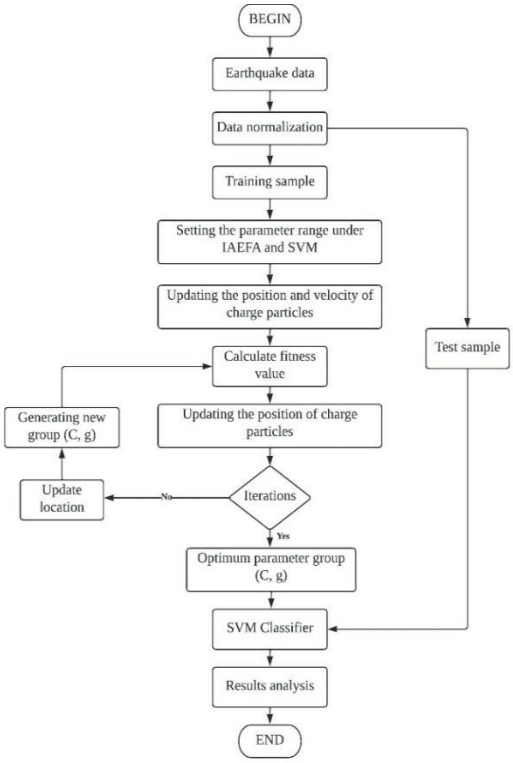

Figure 12: The flow chart of seismic sand liquefaction evaluation based on IAEFA-SVM

SVM is suitable for solving the problem of small sample size, nonlinearity, high latitude, and local minimum. In the SVM model using Radial Basis Function (RBF) as kernel Function, penalty factor C and kernel function g both affect the performance of SVM. The parameters C and G are optimized by using the algorithm. The flow chart of seismic sand liquefaction evaluation based on IAEFA-SVM is shown in Figure 12.

Step 1: Through the 6:4, 7:3, and 8:2 comparison of seismic data, select the 9:1 ratio in the training set and test set and improve the performance of the model. The input variables are the seven parameters shown above.

Step 2: Set the range of values for C and g and the specific parameters for IAEFA.

Step 3: Calculate the fitness value of IAEFA-SVM.

Step 4: According to Formula (8) ~ (13), update the position of the particle, calculate the fitness value of the current position, and compare it with the previous fitness value, choose a better one.

Step 5: Select the max of iterations as the end indicator, the optimal values of the IAEFA output are the C and g parameters in the SVM model.

Step 6: Take the obtained C and g parameters into the prediction model for testing, and analyze the results.

Serial number	I	d_w	d_s	σ'_v	$N_{63.5}$	d_{50}	C_u	τ_d/τ'_v	Measured value	Norm	Seed's	IAEFA-SVM
1	7	0.5	1.7	66.0	3	0.16	1.65	0.10	0	0	0	0
2	7	1.1	6.3	100.0	9	0.14	2.80	0.11	0	0	1	0
3	7	0.7	2.3	17	1	0.07	4.00	0.10	0	0	0	0
4	7	1.4	2.3	82.4	2	0.19	1.90	0.80	0	0	0	0
5	8	3.2	7.2	98.9	8	0.13	2.23	0.172	1	0	0	1
6	8	3.1	9.3	78.3	51	0.32	2.46	0.184	1	1	1	1
7	8	2.3	12.3	140.0	13	0.30	2.43	0.203	1	1	1	1
8	8	1.1	9.22	23.4	12	0.11	2.00	0.225	0	0	0	0
9	8	3	5.1	84.2	9	0.20	2.38	0.159	0	0	0	0
10	8	2	3.46	48.6	8	0.31	2.42	0.163	0	1	0	0
11	9	5	13.52	176.7	64	0.13	2.00	0.34	1	1	1	1
12	9	3.5	8.35	78.5	31	0.21	3.15	0.347	1	1	1	1

Table 8: Evaluation results of sand liquefaction by three methods

5.4 Comparison between Seed's simplification method and IAEFA-SVM model and norm

To prove the accuracy of the model, 78 groups of sample data were trained and 12 groups of sample data were evaluated. And they are also compared with the criterion and the results of Seed's simplification method as shown in Table 8.

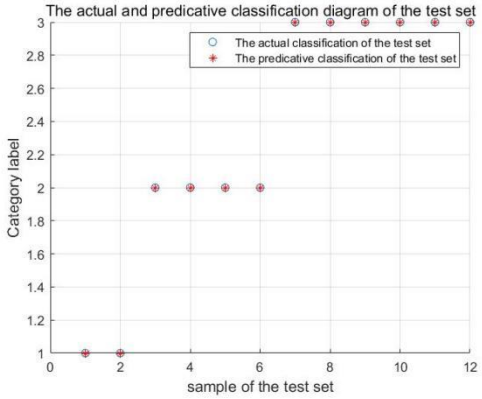

Figure 13: IAEFA-SVM identification diagram

From the comparison results in Table 8, it can be seen that two samples were misjudged by the normalization method and two samples were misjudged by the seed simplification method, the classification accuracy of the IAEFA-SVM model is illustrated. The reason for the error of the standard method is that the method does not take into account some key factors that affect the liquefaction of sand. The reason for the error of the seed simplification method is that it is the empirical discriminant of statistics, and it will have some deviation. It is affected seriously by human factors and has certain limitations.

From the identification diagram as depicted in Figure 13, it can be seen that the accuracy of identifying the degree of sand liquefaction by using the IAEFA-SVM model is 100%. Although there are some differences in the process of (C, g) parameter optimization with IAEFA, it is caused by the randomness of IAEFA in the process of optimization and it does not affect the accuracy of the model. It is proved that the classification effect of IAEFA-SVM is good and it can effectively solve the problem of earthquake liquefaction prediction of sand soil.

6 Conclusion

Based on the analysis of the iterative optimization process of the artificial electric field algorithm, the chaotic strategy is proposed to improve the initial population quality, and the opposite learning strategy and greedy strategy are used to enhance the ability of the algorithm to prevent the local optimal solution.

In the process of benchmark function quota optimization, the results prove the effectiveness of the improved strategy. Based on the analysis of standard deviation results, the IAEFA algorithm can find the theoretical optimal value in 7 out of 9 test functions, the standard deviation of 7 out of 9 test functions is zero, which shows that IAEFA keeps good robustness and has little fluctuation in the iterative process. According to the analysis of the average results, all the six test functions of IAEFA are zero, which shows that the quality of the feasible solution and the search precision of IAEFA can be improved obviously by introducing the opposition-based learning strategy.

Based on the measured data of the earthquake, the seven measured characteristic indexes include intensity, effective overlying pressure, groundwater level, blow counts of SPT, average grain diameter, asymmetrical coefficient, and the shear-to-stress ratio. These characteristics are used as the discriminant indexes of the IAEFA-SVM model. The standard method, seed simplification method, and IAEFA-SVM model were used to distinguish sand liquefaction. In 12 groups of samples, both the standard method and seed simplification method made two misjudges. The accuracy of IAEFA-SVM to identify sand liquefaction reached 100%, providing a new method for the identification of sand liquefaction.

References

[1] Yadav, A. (2019). AEFA: Artificial electric field algorithm for global optimization. *Swarm and Evolutionary Computation*, *48*, 93-108. *https://doi.org/10.1016/j.swevo.2019.03.013*

[2] Demirören, A., Ekinci, S., Hekimoğlu, B., & Izci, D. (2021). Opposition-based artificial electric field algorithm and its application to FOPID controller design for unstable magnetic ball suspension system. *Engineering Science and Technology, an International Journal*, *24*(2), 469-479. *https://doi.org/10.1016/j.jestch.2020.08.001*

[3] Yadav, A. (2020). Discrete artificial electric field algorithm for high-order graph matching. *Applied Soft Computing*, *92*, 106260. *https://doi.org/10.1016/j.asoc.2020.106260*

[4] Yadav, A., & Kumar, N. (2020). Artificial electric field algorithm for engineering optimization problems. *Expert Systems with Applications*, *149*, 113308. *https://doi.org/10.1016/j.eswa.2020.113308*

[5] Hassan, M. H., Kamel, S., El-Dabah, M. A., Khurshaid, T., & Domínguez-García, J. L. (2021). Optimal reactive power dispatch with time-varying demand and renewable energy uncertainty using Rao-3 algorithm. *IEEE Access*, *9*, 23264-23283. *https://ieeexplore.ieee.org/document/9344706*

[6] Sheikh, K. H., Ahmed, S., Mukhopadhyay, K., Singh, P. K., Yoon, J. H., Geem, Z. W., & Sarkar, R. (2020). EHHM: Electrical harmony based hybrid meta-heuristic for feature selection. *IEEE Access*, *8*,

158125-158141.
https://ieeexplore.ieee.org/document/9178740

[7] Xu, H., Zhai, X., Wang, Z., Cui, Z., Fu, Z., & Lu, Y. (2019). An epitaxial synaptic device made by a band-offset BaTiO3/Sr2IrO4 bilayer with high endurance and long retention. *Applied Physics Letters*, *114*(10), 102904.
https://doi.org/10.1063/1.5085126

[8] Singh, P. K., & Sharma, A. (2022). An intelligent WSN-UAV-based IoT framework for precision agriculture application. *Computers and Electrical Engineering*, *100*, 107912.
https://doi.org/10.1016/j.compeleceng.2022.107912

[9] Zeng, H., Dhiman, G., Sharma, A., Sharma, A., & Tselykh, A. (2021). An IoT and Blockchain-based approach for the smart water management system in agriculture. *Expert Systems*, e12892.
https://doi.org/10.1111/exsy.12892

[10] Sharma, A., & Singh, P. K. (2021). UAV-based framework for effective data analysis of forest fire detection using 5G networks: An effective approach towards smart cities solutions. *International Journal of Communication Systems*, e4826.
https://doi.org/10.1002/dac.4826

[11] Sharma, A., Singh, P. K., & Kumar, Y. (2020). An integrated fire detection system using IoT and image processing technique for smart cities. *Sustainable Cities and Society*, *61*, 102332.
https://doi.org/10.1016/j.scs.2020.102332

[12] Tizhoosh, H. R. (2005, November). Opposition-based learning: a new scheme for machine intelligence. In *International conference on computational intelligence for modelling, control and automation and international conference on intelligent agents, web technologies and internet commerce (CIMCA-IAWTIC'06)* (Vol. 1, pp. 695-701). IEEE.
https://ieeexplore.ieee.org/document/1631345/

[13] Karimi, F., Attarpour, A., Amirfattahi, R., & Nezhad, A. Z. (2019). Computational analysis of non-invasive deep brain stimulation based on interfering electric fields. *Physics in Medicine & Biology*, *64*(23), 235010.
10.1088/1361-6560/ab5229

[14] Hashim, F. A., Hussain, K., Houssein, E. H., Mabrouk, M. S., & Al-Atabany, W. (2021). Archimedes optimization algorithm: a new metaheuristic algorithm for solving optimization problems. *Applied Intelligence*, *51*(3), 1531-1551.
https://doi.org/10.1007/s10489-020-01893-z

[15] Alsattar, H. A., Zaidan, A. A., & Zaidan, B. B. (2020). Novel meta-heuristic bald eagle search optimisation algorithm. *Artificial Intelligence Review*, *53*(3), 2237-2264.
https://doi.org/10.1007/s10462-019-09732-5

[16] Sayed, G. I., Khoriba, G., & Haggag, M. H. (2018). A novel chaotic salp swarm algorithm for global optimization and feature selection. *Applied Intelligence*, *48*(10), 3462-3481.
https://doi.org/10.1007/s10489-018-1158-6

[17] Ge, Q., Li, A., Li, S., Du, H., Huang, X., & Niu, C. (2021). Improved Bidirectional RRT Path Planning Method for Smart Vehicle. *Mathematical Problems in Engineering*, *2021*.
https://doi.org/10.1155/2021/6669728

[18] Jeong, W., Jeong, S. M., Lim, T., Han, C. Y., Yang, H., Lee, B. W., & Ju, S. (2019). Self-emitting artificial cilia produced by field effect spinning. *ACS applied materials & interfaces*, *11*(38), 35286-35293.
https://doi.org/10.1021/acsami.9b09571

[19] Petwal, H., & Rani, R. (2020). An improved artificial electric field algorithm for multi-objective optimization. *Processes*, *8*(5), 584.
https://doi.org/10.3390/pr8050584

[20] Selem, S. I., El-Fergany, A. A., & Hasanien, H. M. (2021). Artificial electric field algorithm to extract nine parameters of triple-diode photovoltaic model. *International Journal of Energy Research*, *45*(1), 590-604.
https://doi.org/10.1002/er.5756

[21] Naderipour, A., Abdul-Malek, Z., Mustafa, M. W. B., & Guerrero, J. M. (2021). A multi-objective artificial electric field optimization algorithm for allocation of wind turbines in distribution systems. *Applied Soft Computing*, *105*, 107278.
https://doi.org/10.1016/j.asoc.2021.107278

[22] Yadav, A. (2021). An intelligent model for the detection of white blood cells using artificial intelligence. *Computer methods and programs in biomedicine*, *199*, 105893.
https://doi.org/10.1016/j.cmpb.2020.105893

[23] Sharma, A., & Jain, S. K. (2021). Day-ahead optimal reactive power ancillary service procurement under dynamic multi-objective framework in wind integrated deregulated power system. *Energy*, *223*, 120028.
https://doi.org/10.1016/j.energy.2021.120028

[24] Wang, H., Sharma, A., & Shabaz, M. (2022). Research on digital media animation control technology based on recurrent neural network using speech technology. International Journal of System Assurance Engineering and Management, 13(1), 564-575.
https://doi.org/10.1007/s13198-021-01540-x

[25] Sharma, P., Mishra, A., Saxena, A., & Shankar, R. (2021). A novel hybridized fuzzy PI-LADRC based improved frequency regulation for restructured power system integrating renewable energy and electric vehicles. *IEEE Access*, *9*, 7597-7617.
https://ieeexplore.ieee.org/document/9312597

[26] Alihodzic, A., Mujezinovic, A., & Turajlic, E. (2021). Electric and Magnetic Field Estimation Under Overhead Transmission Lines Using Artificial Neural Networks. *IEEE Access*, *9*, 105876-105891.
10.1109/ACCESS.2021.3099760

[27] Chen, M., Sharma, A., Bhola, J., Nguyen, T. V., &

Truong, C. V. (2022). Multi-agent task planning and resource apportionment in a smart grid. International Journal of System Assurance Engineering and Management, 13(1), 444-455. *https://doi.org/10.1007/s13198-021-01467-3*

[28] Kharrich, M., Kamel, S., Abdeen, M., Mohammed, O. H., Akherraz, M., Khurshaid, T., & Rhee, S. B. (2021). Developed approach based on equilibrium optimizer for optimal design of hybrid PV/Wind/Diesel/Battery microgrid in Dakhla, Morocco. *IEEE Access*, *9*, 13655-13670. *10.1109/ACCESS.2021.3051573*

[29] Chen, Y., Zhang, W., Dong, L., Cengiz, K., & Sharma, A. (2021). Study on vibration and noise influence for optimization of garden mower. Nonlinear Engineering, 10(1), 428-435. *https://doi.org/10.1515/nleng-2021-0034*

[30] Youd, T. L., & Idriss, I. M. (2001). Liquefaction resistance of soils: summary report from the 1996 NCEER and 1998 NCEER/NSF workshops on evaluation of liquefaction resistance of soils. *Journal of geotechnical and geoenvironmental engineering*, *127*(4), 297-313. *https://doi.org/10.1061/(ASCE)1090-0241(2001)127:4(297)*

[31] Chopra, S., Dhiman, G., Sharma, A., Shabaz, M., Shukla, P., & Arora, M. (2021). Taxonomy of adaptive neuro-fuzzy inference system in modern engineering sciences. *Computational Intelligence and Neuroscience*, *2021*. *https://doi.org/10.1155/2021/6455592*

[32] Zhan, X., Mu, Z. H., Kumar, R., & Shabaz, M. (2021). Research on speed sensor fusion of urban rail transit train speed ranging based on deep learning. Nonlinear Engineering, 10(1), 363-373. *https://doi.org/10.1515/nleng-2021-0028*

[33] Han, Z., Chen, M., Shao, S., & Wu, Q. (2022). Improved artificial bee colony algorithm-based path planning of unmanned autonomous helicopter using multi-strategy evolutionary learning. *Aerospace Science and Technology*, *122*, 107374. *https://doi.org/10.1016/j.ast.2022.107374*

[34] Liu, C., Lin, M., Rauf, H. L., & Shareef, S. S. (2021). Parameter simulation of multidimensional urban landscape design based on nonlinear theory. Nonlinear Engineering, 10(1), 583-591. *https://doi.org/10.1515/nleng-2021-0049*

[35] Sharma, A., Singh, P. K., Hong, W. C., Dhiman, G., & Slowik, A. (2021). Introduction to the Special Issue on Artificial Intelligence for Smart Cities and Industries. Scalable Computing: Practice and Experience, 22(2), 89-91. *https://doi.org/10.12694/scpe.v22i2.1939*

[36] Wang, H., Wu, Z., Rahnamayan, S., Sun, H., Liu, Y., & Pan, J. S. (2014). Multi-strategy ensemble artificial bee colony algorithm. *Information Sciences*, *279*, 587-603. *https://doi.org/10.1016/j.ins.2014.04.013*

[37] Lu, H., Sun, S., Cheng, S., & Shi, Y. (2021). An adaptive niching method based on multi-strategy fusion for multimodal optimization. *Memetic Computing*, *13*(3), 341-357. *https://doi.org/10.1007/s12293-021-00338-5*

[38] Zhang, X., Rane, K. P., Kakaravada, I., & Shabaz, M. (2021). Research on vibration monitoring and fault diagnosis of rotating machinery based on internet of things technology. Nonlinear Engineering, 10(1), 245-254. *https://doi.org/10.1515/nleng-2021-0019*

[39] Sharma, A., Georgi, M., Tregubenko, M., Tselykh, A., & Tselykh, A. (2022). Enabling Smart Agriculture by Implementing Artificial Intelligence and Embedded Sensing. Computers & Industrial Engineering, 107936. *https://doi.org/10.1016/j.cie.2022.107936*

[40] Zhuang, D. Y., Ma, K., Tang, C. A., Liang, Z. Z., Wang, K. K., & Wang, Z. W. (2019). Mechanical parameter inversion in tunnel engineering using support vector regression optimized by multi-strategy artificial fish swarm algorithm. *Tunnelling and underground space technology*, *83*, 425-436. *https://doi.org/10.1016/j.tust.2018.09.027*